Improving the Electrical Conductivity of the Composite Comprising Bismuth Oxide, Activated Carbon, and Graphite for Use as a Battery Anode

Yayuk Astuti*, Faradina Azahra Zaqia, Aulia Zahra Ekaningsih, Gunawan Gunawan, and Adi Darmawan

Department of Chemistry, Faculty of Science and Mathematics, Diponegoro University, Jl. Prof. Soedharto SH, Tembalang, Semarang 50275, Indonesia

* ***Corresponding author:***

email: yayuk.astuti@live.undip.ac.id

Received: April 17, 2022
Accepted: June 13, 2023

DOI: 10.22146/ijc.74155

Abstract: *This research is concerned with the synthesis and characterization of a composite material that may be used as a battery electrode. Bismuth oxide (Bi_2O_3) was synthesized from $Bi(NO_3)_3{\cdot}5H_2O$, Na_2SO_4, and NaOH mixed with commercial activated carbon and graphite. The composite formation process was carried out using the hydrothermal method at 110 °C for 5 h. The characterization data indicated the composites produced contained Bi_2O_3 with a monoclinic crystal system, and Bi_2O_3 particles were evenly distributed in the composite. The composites were characterized to be mesoporous, with the electrical conductivity reaching 10^{-1} S m^{-1}. The development of this composite material has potential applications in the field of energy storage, particularly in the development of battery anode.*

Keywords: *bismuth oxide; commercial activated carbon; graphite doping; battery anode*

■ INTRODUCTION

Batteries are widely regarded as the most efficient and convenient power source for electronic devices, thanks to their adaptable structure and extended operational duration. They operate by transforming chemical energy from their active components into electrical energy through electrochemical reactions [1]. A good indicator of a working battery is the electrochemical cycle performance, which depends on the materials comprising the anode. Materials that are used as anodes must have good charge or ionic conductivity characteristics (> 10^3 S cm^{-1}), large energy capacity, high coulomb output (A h g^{-1}), high effectiveness as a reducing agent, excellent stability, straightforward manufacturing, and affordability [1].

Bismuth oxide (Bi_2O_3) is a promising candidate for utilization as a battery anode due to its favorable electrochemical stability, strong redox reversibility, and substantial capacity, as demonstrated in recent research [2-4]. Notably, Bi_2O_3 boasts a volumetric capacity of 3765 mA h cm^{-3}, a potential difference of 2.8 V, and it offers the additional advantages of being non-toxic and cost-effective [5]. However, in using Bi_2O_3 as an anode, an issue of low electrical conductivity value [6-7] that inhibits the conductivity of electrons in the battery needs to be overcome. This can be done through the addition of other materials, namely commercial activated carbon and graphite, which can increase electrical conductivity.

Utilizing commercially produced activated carbon sourced from coconut shells results in the creation of carbon materials characterized by minimal internal resistance and excellent electrical conductivity, as evidenced in reference [8]. These carbons offer substantial volumetric capacity and a significant potential difference, as indicated in reference [9]. In contrast, graphite exhibits remarkable electrical conductivity, a high energy density (implying a high specific capacity), and an exceptionally long cycle life [10]. Some researchers reported the electrical conductivity of graphite depends on the humidity [11] and grain composition [12]. Said characteristics of activated carbon and graphite are expected to be able to promote Bi_2O_3 ability as a battery anode.

Astuti et al. [13] conducted research on the synthesis and characterization of Bi_2O_3/activated carbon

composite for battery anode. They employed the hydrothermal method with varying weight ratios of activated carbon to bismuth nitrate pentahydrate, specifically 2:1, 1:1, and 1:2. In their findings, the electrical conductivities were measured at 0.59×10^{-5}, 1.24×10^{-5}, and 0.51×10^{-5} Sm^{-1} for the respective ratios. These conductivity values are relatively low. It is plausible that the composite had not yet achieved optimal Bi_2O_3 formation, and carbon distribution appeared to be more dominant than Bi_2O_3 within the material.

Hence, there is a need to refine the synthesis process to create an improved Bi_2O_3/activated carbon composite with a more precise composition. To date, no prior research has explored the synthesis of a composite consisting of Bi_2O_3, activated carbon, and graphite. This current study aims to fill this research gap and hopes to offer valuable insights into the potential applications of metal oxide and carbon-based composites in electrode technology.

■ EXPERIMENTAL SECTION

Materials

The substances employed in this investigation encompassed $Bi(NO_3)_3{\cdot}5H_2O$ from Sigma Aldrich, distilled water, 60% H_3PO_4 (v/v), Na_2SO_4 powder, NaOH crystal sourced from Merck, as well as commercially available activated carbon (AC) and graphite.

Instrumentation

The instrumentations used in this research were Fourier transform infrared (Shimadzu IRAffinity-1), X-ray diffraction (XRD, Shimadzu 7000), scanning electron microscope (SEM, Jeol JED 6510LA model), thermogravimetric analysis (TGA, Mettler Toledo TGA/DSC 3+), gas sorption analysis (GSA, Tristar II 3020) and LCR meter (HIOKI 3532-50).

Procedure

Synthesis of Bi_2O_3/AC/graphite composite

A total of 8 mmol of $Bi(NO_3)_3{\cdot}5H_2O$ was combined with 12 mmol of Na_2SO_4, which were then dissolved in 40 mL of distilled water and stirred using a magnetic stirrer (IKA RH Basic KT/C) at 1500 rpm for 45 min. The solution was agitated using a magnetic stirrer (IKA RH Basic KT/C) at 1500 rpm for 45 min. Subsequently, 40 mL of a 72 mmol NaOH solution [14] was added to the mixture. To this blend, 0.5 g of commercially available AC and 0.1 g of graphite were introduced. The resulting mixture was then introduced into a hydrothermal reactor and subjected to a temperature of 110 °C for a duration of 5 h. During this process, the reactants within the sealed container were heated by rapidly increasing temperature and pressure generated by water [6,15]. The temperature and pressure exerted by the water played a crucial role in facilitating the formation of the composite. Following the hydrothermal treatment, the mixture was cooled and subsequently filtered. The precipitate obtained from the filtration was dried in an oven (Fisher Scientific) at 110 °C for 60 min and subsequently sieved to a 100-mesh size. The same procedure was replicated for the synthesis of composites with varying amounts of $Bi(NO_3)_3{\cdot}5H_2O$, specifically 24 and 32 mmol. Accordingly, the composites synthesized with 8, 24, and 32 mmol of Bi_2O_3 in conjunction with commercial AC and graphite were designated as BCG1, BCG2, and BCG3, respectively.

Characterization of the Bi_2O_3/AC/graphite composite material

The resultant composite materials of Bi_2O_3, AC, and graphite underwent a series of characterization processes. FTIR analysis was conducted to elucidate the functional groups present in the composites. FTIR measurements were carried out in the spectral range of 4000 to 400 cm^{-1}, with a scanning rate of 0.25 cm^{-1}, all at room temperature. Furthermore, the composites underwent XRD analysis to identify their crystalline structures. This analysis was performed by measuring 2θ angles with Cu-Kα radiation (λ = 0.15406 nm). The surface morphology and the spatial distribution of Bi_2O_3 and AC within the composite were assessed using a SEM. This analysis was conducted at magnifications of 100× and 5000× and was complemented by mapping and energy dispersive X-ray (EDX) analysis. Thermal decomposition and stability of the composite materials were investigated through TGA and differential thermogravimetric analysis (DTG). The samples were subjected to a temperature range of 40–800 °C at a

heating rate of 4 °C/min under a nitrogen (N_2) atmosphere. To assess the size and distribution of pores within the composites, GSA was conducted. This analysis involved the use of N_2 gas. Lastly, the conductivity of the composites was determined through LCR characterization. The samples were prepared in pellet form, with a diameter of 1.5 cm and a thickness ranging from 2 to 5 mm.

■ RESULTS AND DISCUSSION

Preparation of Graphite Doped Bi_2O_3/AC Composite

The synthesis of the composite consisting of Bi_2O_3, commercial AC, and graphite, with varying mole ratios of bismuth nitrate pentahydrate, was initiated by carrying out a reaction involving the precursor compounds $Bi(NO_3)_3{\cdot}5H_2O$, Na_2SO_4, and NaOH. This procedure closely followed the protocol outlined by Wu et al. [14]. Subsequently, commercial AC and graphite were introduced into the solution, followed by thorough homogenization, before subjecting the mixture to hydrothermal heating. The formation mechanism of Bi_2O_3, as proposed by Wu et al. [14] underpinned Eq. (1).

$$\begin{aligned} 2Bi(NO_3)_3 \cdot 5H_2O + Na_2SO_4 &\rightarrow Bi_2O(OH)_2SO_4 + 2NaNO_3 \\ &\quad + 4HNO_3 + 7H_2O \\ Bi_2O(OH)_2SO_4 + 2NaOH + H_2O &\rightarrow 2Bi(OH)_3 + Na_2SO_4 \\ 2Bi(OH)_3 &\rightarrow Bi_2O_3 + 3H_2O \end{aligned} \quad (1)$$

The BCG1 composite product had grayish-black powder form, while the BCG2 and BCG3 composites showed gray color. The BCG3 had an agglomerated appearance, as shown in Fig. 1. The resulting coloration of the material exhibited a gray hue, which emerged as a result of the combination of the pale-yellow tint contributed by Bi_2O_3 [16] and the black color imparted by the presence of AC and graphite.

Material Characterization

Functional group structure

FTIR characterization was conducted to determine the functional groups present in the composite sample. The FTIR spectra of the composite samples, along with pure Bi_2O_3, commercial AC, and graphite, are shown in Fig. 2. Fig. 2 presents the FTIR spectra of commercial AC, having absorption at wavenumbers of 1600–1475 cm^{-1}, denoting the C=C group [18] and 1320–1000 cm^{-1}, denoting C–O group [19]. In the absorption spectra for graphite, the presence of a C=C group is indicated at wavenumber 1633 cm^{-1} [20]. Similar absorptions were also shown by each composite sample, with the C=C group in the absorption area of about 1626 and 1642 cm^{-1} and the C–O group in the absorption area of about 1103 cm^{-1}.

The above data present that the three composite samples have almost the same pattern of absorptions with the presence of a fairly sharp absorption in the area

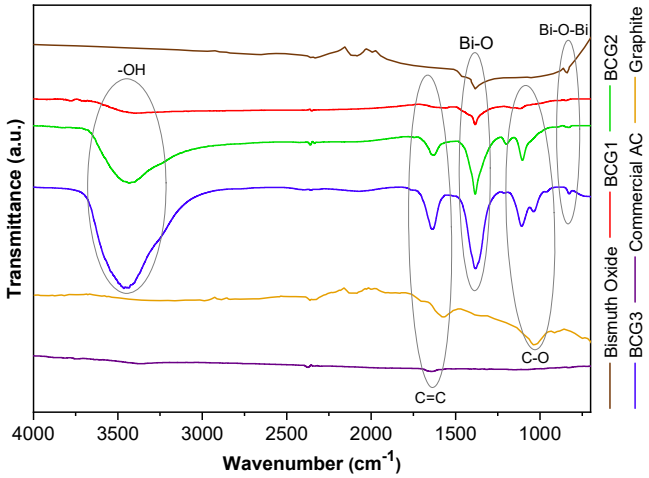

Fig 2. FTIR spectra of composite products, pure bismuth oxide [17], commercial AC [15], and graphite [15]

Fig 1. Composite products (a) BCG1, (b) BCG2, and (c) BCG3

around 820–842 cm^{-1}, indicating the Bi–O–Bi group and the absorption in the area around 1383 cm^{-1}, which indicates the Bi–O group. The same absorption was also shown by the pure Bi_2O_3 samples [13], i.e., the absorption of Bi–O–Bi groups in the 829 cm^{-1} area [21], and at the wavenumber of about 1380 cm^{-1}, showing the presence of a Bi–O group [13,22]. This implies that Bi_2O_3 was formed in each composite sample. Additionally, the three composite samples contain O–H groups observed at the wavenumber of about 3400 cm^{-1} [23]. It is expected due to the by-product and imperfect reaction as presented in Eq. (1). The three composite samples had the same group absorption, however, with different intensities. The comprehensive data pertaining to the functional groups present in the three composite products, namely pure Bi_2O_3, commercial AC, and graphite, as determined through FTIR testing, are detailed in Table 1.

Crystal structure

Characterization of composite samples using XRD was carried out to determine the success of the formation of Bi_2O_3 in the composite and to determine the crystal structure of Bi_2O_3 in the composite. The results of the XRD diffractograms of all the composites made and the comprising components can be seen in Fig. 3. The XRD characterization results (Fig. 3) show that the diffractogram of the BCG1 composite has a notable match with the α-Bi_2O_3 diffractogram. The BCG1 composite has high peak 2θ values at 27.386°, 33.248°, and 46.309°. The 2θ values are almost similar to the 2θ values of α-Bi_2O_3 peaks at 27.377°, 33.039°, and 46.305° (JCPDS no. 41-1449).

Table 1. Functional groups identification from the FTIR analysis

Functional group	Wavenumber (cm^{-1})					
	Sample			Bismuth oxide	Commercial activated carbon	Graphite
	BCG1	BCG2	BCG3			
Bi–O	1383.54	1383.61	1383.07	1400–1300	-	-
Bi–O–Bi	842.50	841.60	820.60	900–700	-	-
C–O	1103.39	1104.09	1108.28	-	1032.86	-
C=C	1626.10	1637.36	1630.14	-	1570.01	1642.90
–OH	3399.10	3433.74	3464.66	-	-	-

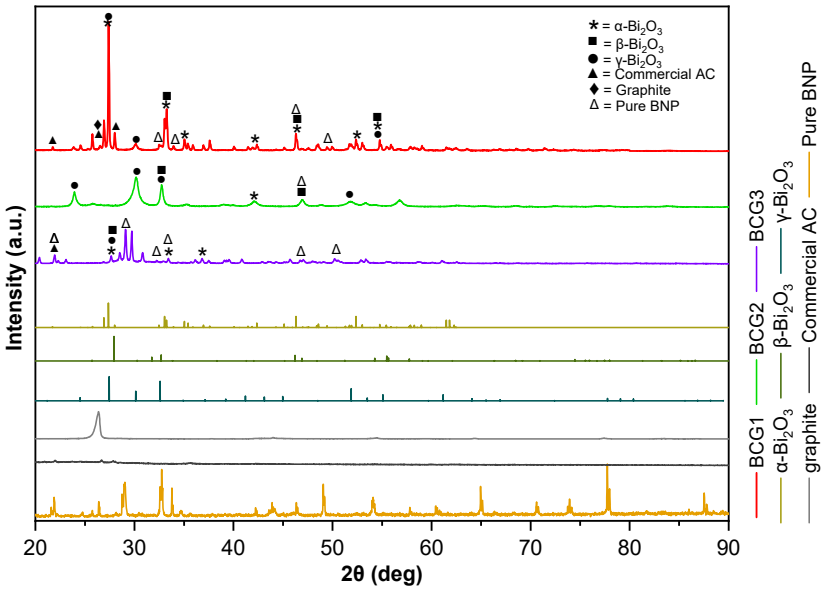

Fig 3. Diffractograms of composite products, Bi_2O_3 (JCPDS), bismuth nitrate pentahydrate [6], commercial AC [15], and graphite [15]

The BCG2 composite diffractogram shows that there are sharp peaks that are almost similar to the cubic crystal system (γ-Bi_2O_3), though at low intensity, namely at 2θ values of 30.159°, 32.746°, and 51.788° (JCPDS no. 27-0052). The sharp but low-intensity peaks indicate that Bi_2O_3 with a cubic crystal system (γ-Bi_2O_3) may have been formed but to a small degree. Wu et al. [14] on the XRD diffractogram of the by-product (Eq. (1)) in the form of $Bi_2(OH)_2SO_4$ presented sharp peaks at the value of 2θ around 30.159° to 32.746°, similar to the composite. The diffractogram results indicate that the BCG2 composite still has residual reaction by-products in the form of $Bi_2(OH)_2SO_4$, meaning that less Bi_2O_3 was produced.

The BCG3 composite diffractogram shows the presence of sharp peaks with considerable intensity at the 2θ values of 21.941°, 29.099°, 32.904°, and 33.425°, which matched the bismuth nitrate pentahydrate diffractogram peaks. These peaks are also thought to be the peaks of the by-product $Bi_2(OH)_2SO_4$ + $Bi(OH)_3$ [14] formed during the reaction (Eq. (1)). The BCG3 composite diffractogram also displays small peaks at 27.651°, 33.425°, and 36.824° having a good match with the α-Bi_2O_3 diffractogram (JCPDS no. 41-1449), indicating that the BCG3 composite contained more $Bi(NO_3)_3{\cdot}5H_2O$ (BNP) precursor and reaction by-products compared to Bi_2O_3.

Morphology and particle distribution

In Fig. 4, it can be observed that the BCG1 composite exhibited a morphology characterized by rod-shaped particles, with lengths ranging from 6.6 to 11.2 μm and widths spanning 1.4 to 2.4 μm. This rod-like particle structure is indicative of the presence of Bi_2O_3 within the composite, consistent with findings reported by Wu et al. [14]. Meanwhile, the BCG2 composite showed irregular particle shapes, with few that were shaped like rods with a length ranging from 14–35 μm and a width between 4–9 μm. Alternatively, the BCG3 composite showed particles having irregular shapes and agglomeration, with a length between 2–5.4 μm and a width of about 1–4 μm. Furthermore, Fig. 5 presents the SEM mapping images of the three composite samples.

In Fig. 5, the distribution of elements, including bismuth (Bi), carbon (C), oxygen (O), and silicon (Si), within the BCG1, BCG2, and BCG3 composites is depicted. These elements are denoted by the colors red, green, yellowish green, and blue, respectively. It is evident that in the BCG1 composite, the distribution of Bi and C appears relatively balanced and evenly spread across the material's surface. In the case of BCG2, the surface is noticeably dominated by the presence of the Bi element.

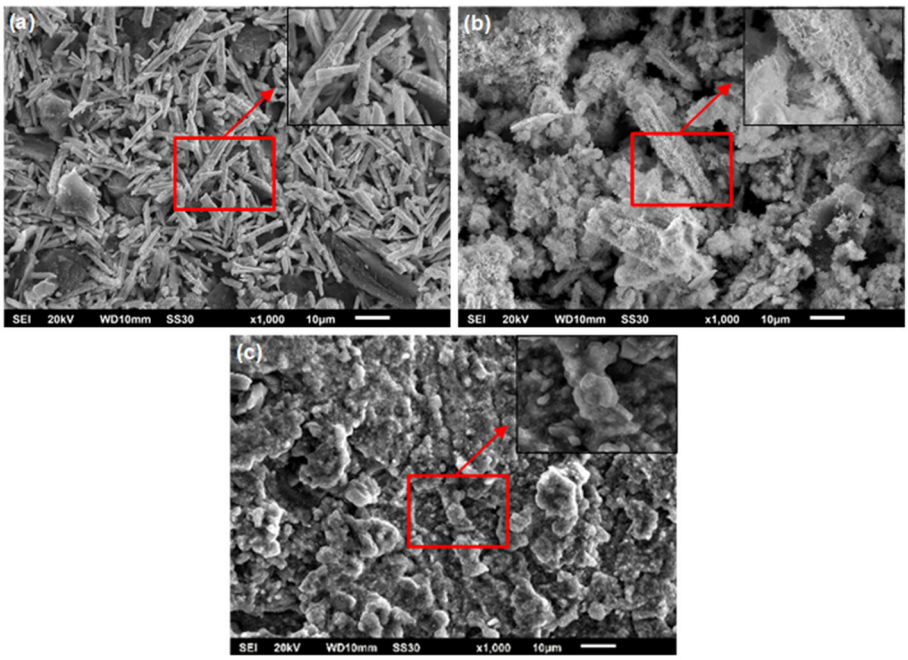

Fig 4. SEM images of composites (a) BCG1, (b) BCG2, and (c) BCG3

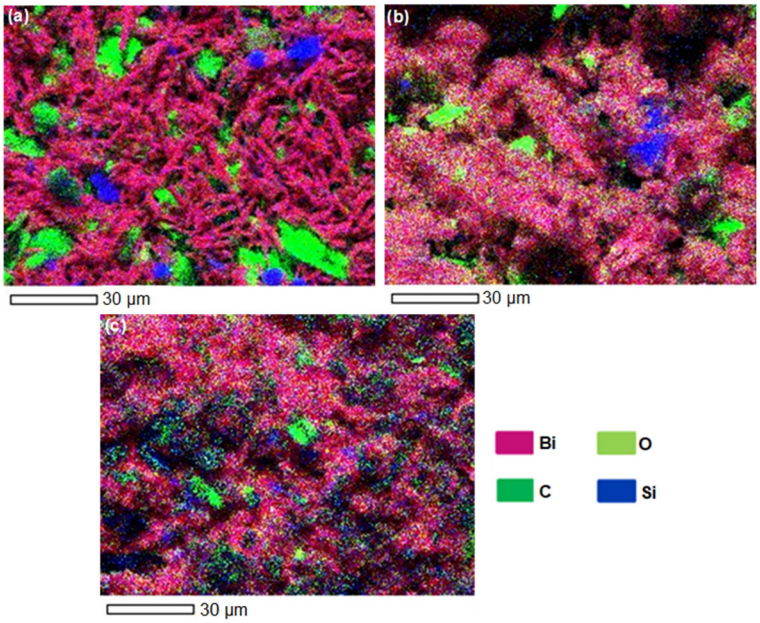

Fig 5. Mapping images of composites (a) BCG1, (b) BCG2, and (c) BCG3

Conversely, in BCG3, both Bi and O elements are prevalent on the sample surface, making the presence of C less conspicuous. The EDX data presented in Fig. 6 corroborates the distribution patterns of these elements.

Based on the EDX results shown in Fig. 6, the three composite samples contained elements such as C, Bi, O, and a small amount of Na and Si. The C element indicated the presence of carbon in the composite. The Bi and O elements in BCG1 originated from Bi_2O_3 formed, as suggested by the XRD results (Fig. 3). The presence of a small amount of Na is thought to have come from the remaining precursor (NaOH), whereas the Si element is assumed to have come from the activated carbon. The elements in the BCG2 composite are thought to have originated from the precursor materials and reaction by-products, as per the XRD data where the Bi_2O_3 formed in BCG2 was very small. Furthermore, in the EDX results of the BCG3 composite, in addition to the C, Bi, O, Na, and Si elements, the elements of N, P, and S were also present. Elements such as Bi, O, N, Na, and S are thought to have come from Eq. (1) by-product or the left-over precursors as indicated by the XRD results (Fig. 3). Overall, the C element decreased in amount with increasing mole variation of BNP, causing the distribution of the C element to be increasingly invisible on the surface of the material in the mapping results shown in Fig. 5.

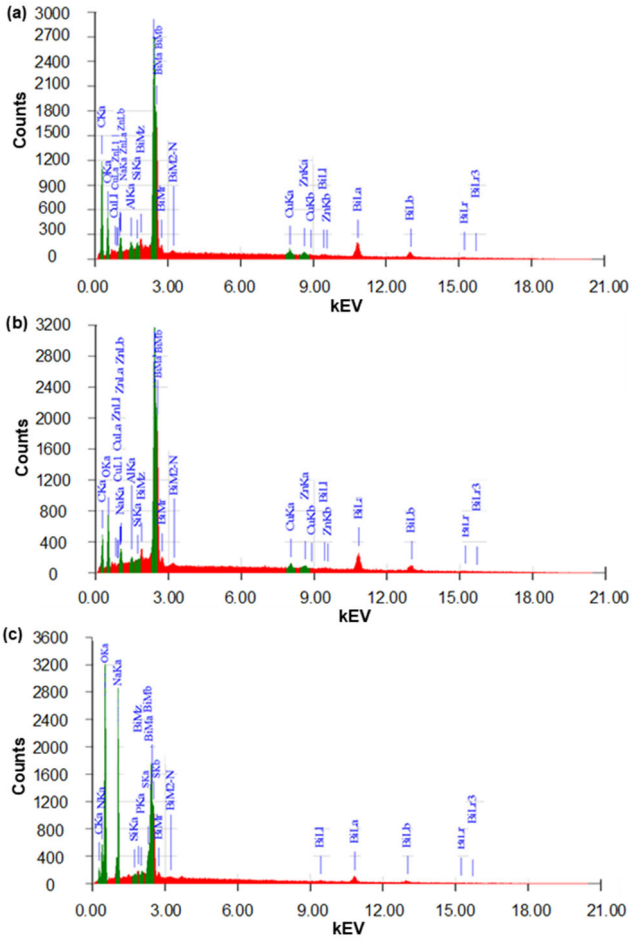

Fig 6. EDX spectra of composites (a) BCG1, (b) BCG2, and (c) BCG3

TGA-DTG composite characterization

TGA-DSC analysis was employed to assess the decomposition mechanism and thermal stability of the composite materials. The TGA-DTG results for these composites are presented in Fig. 7. Based on the results, the composite BCG1 and BCG2 underwent five stages of the decomposition process, while the BCG3 composite experienced four stages of decomposition. Stage I of the three composites occurred at a temperature of 200–310 °C, denoting the removal process of several functional groups such as –COO–, –CO–, and –OH– from graphite [24] as well as materials other than carbon such as cellulose and hemicellulose from AC [25].

In the second stage, which occurred within the temperature range of 250 to 380 °C, it is presumed that the process involved the removal of amorphous residues [26], including substances such as $NaNO_3$, NaOH, and SO_4^{-2}. Notably, in BCG3, there was a more substantial weight loss during this stage in comparison to BCG1 and BCG2. This suggests that the BCG3 composite experienced a greater decomposition of amorphous residues, possibly due to the presence of reaction by-products such as $Bi_2O(OH)_2SO_4$ and the BNP precursor, as indicated by the XRD results (Fig. 3).

Stage III occurred at a temperature range of 300–400 °C, denoting the mass transformation process of the precursors to form Bi_2O_3 [27]. In stage IV, composites undergo a transformation from a monoclinic structure (α-Bi_2O_3) into a body-centered cubic structure (γ-Bi_2O_3) at a temperature of about 500 °C. Stage V indicates the retransformation of the body-centered cubic (γ-Bi_2O_3) structure into the monoclinic structure (α-Bi_2O_3) [28] at

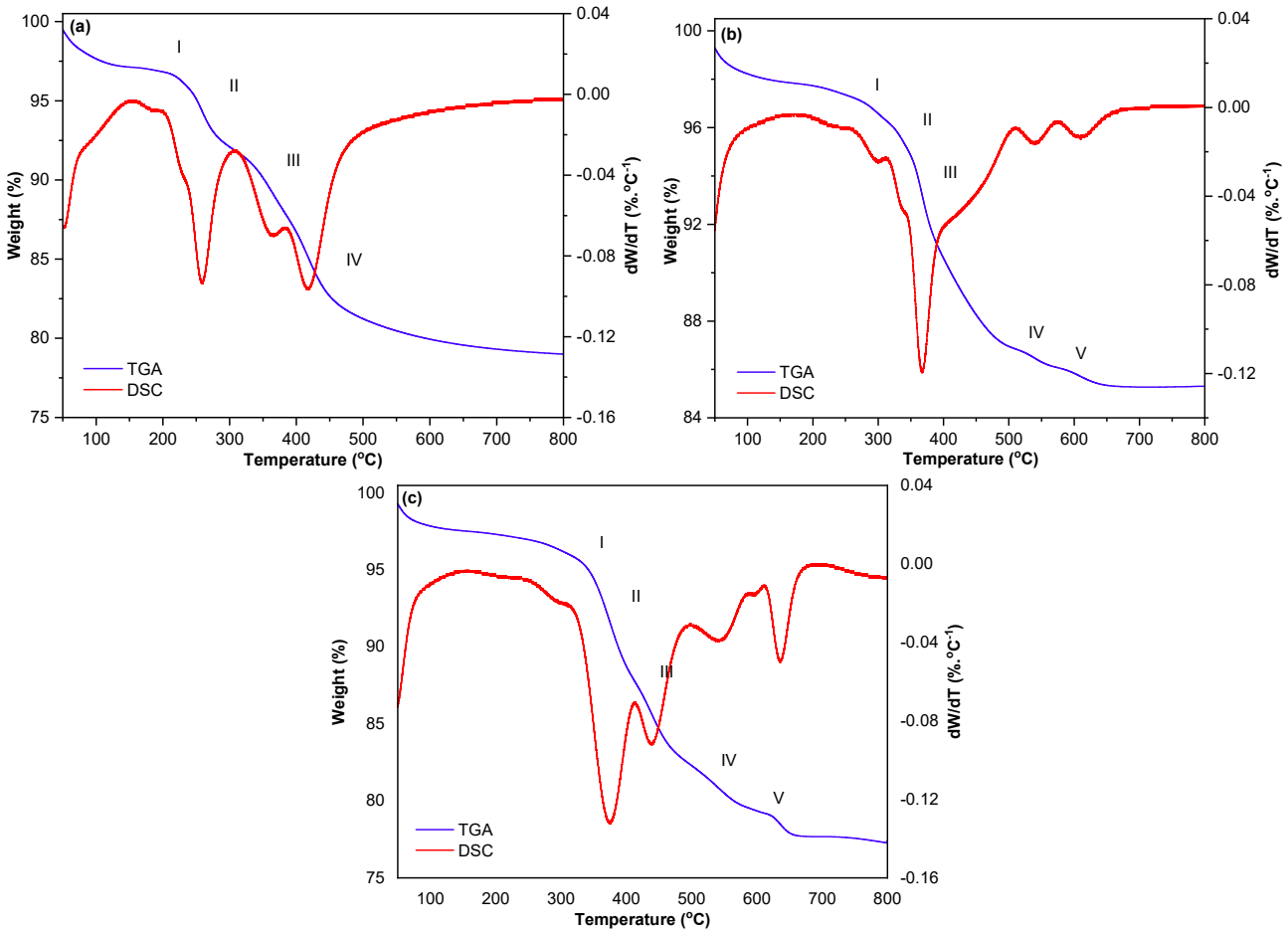

Fig 7. TGA-DTG results of composites (a) BCG1, (b) BCG2, and (c) BCG3

a temperature of about 600 °C. The TG-DTG curves of the three composite samples show that thermal stability was obtained at ≥ 700 °C.

Surface area and pore size

Fig. 8 presented the evidence that the three composite samples exhibit similar isotherm patterns, specifically of type IV, which is characterized by the presence of a hysteresis loop. The presence of this hysteresis pattern signifies that the samples possess a porous nature. The results obtained from GSA analysis for the BCG1, BCG2, and BCG3 composites are summarized in Table 2.

Table 2 reveals that all three composite samples have mesoporous structures, featuring pore radii ranging from 3 to 50 nm [29]. As reported in a study by Agrawal et al. [30] on the production and characterization of nitrogen-doped hard carbon as a battery anode material, porosity plays a significant role in influencing a sample's conductivity. Samples with high porosity, meaning they contain numerous small-sized pores, tend to exhibit lower conductivity due to increased resistance caused by the abundance of small pores. This correlation is supported by the GSA and LCR characterization results for the BCG3 composite, which possesses the largest pore size at 15.168 nm. Interestingly, despite having a small pore volume and surface area (0.011 cm^3/g and 2.792 m^2/g,

Table 2. Surface area and pore size

Sample	S_{BET} (m^2/g)	V_{pore} (cm^3/g)	Pore size (nm)
BCG1	2.311	0.007	12.822
BCG2	5.594	0.016	11.664
BCG3	2.792	0.011	15.168

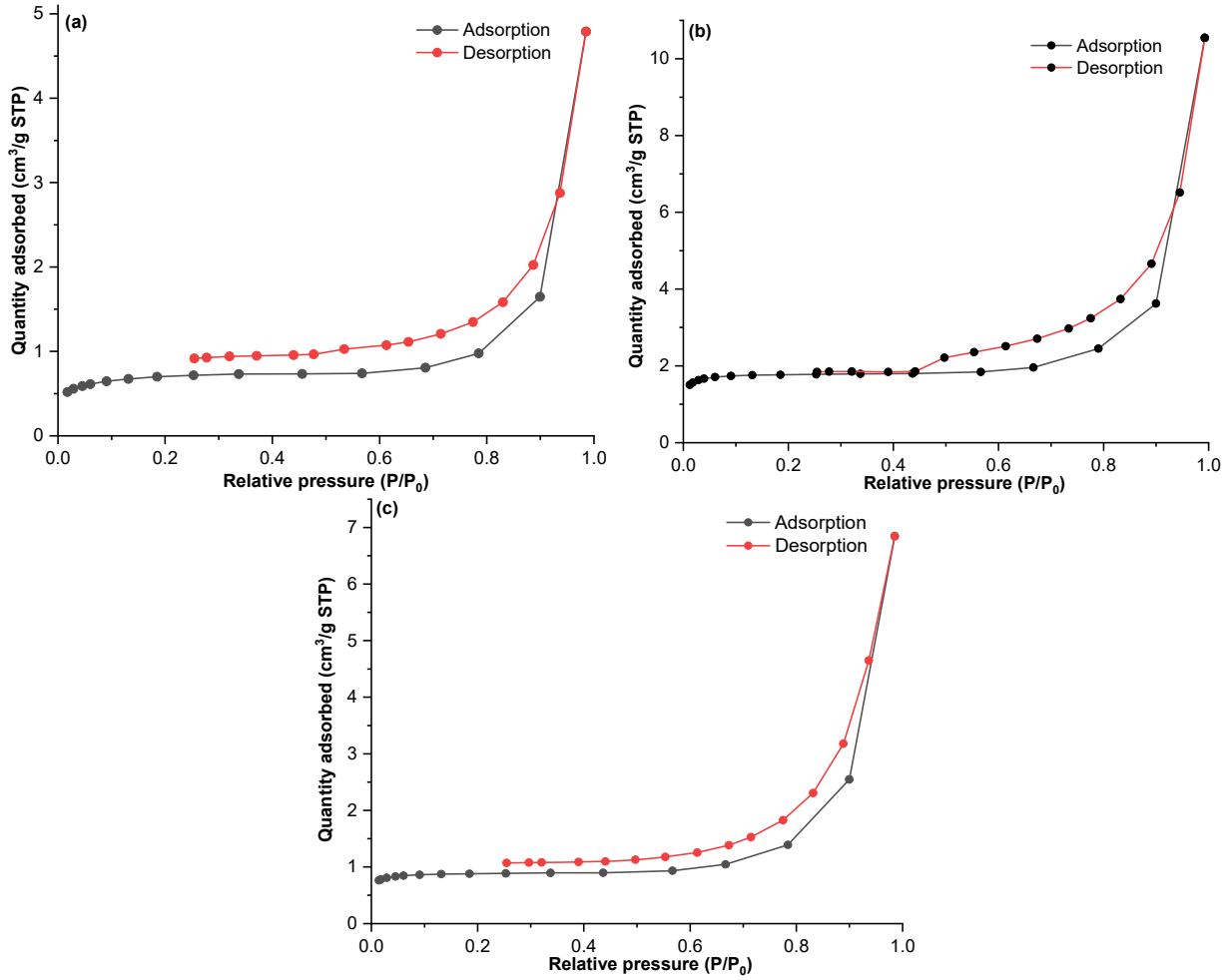

Fig 8. N_2 adsorption/desorption isotherm graphs of composites (a) BCG1, (b) BCG2, (c) BCG3

Table 3. LCR Meter conductivity measurement

Sample	Conductivity value (S m^{-1})
BCG1	0.02×10^{-1}
BCG2	0.01×10^{-1}
BCG3	1.02×10^{-1}
Commercial AC	7.41×10^{-6}
Bi_2O_3 [7]	1.55×10^{-7}
Graphite	4.03×10^{1}

respectively), the BCG3 composite exhibits low measured resistance and high sample conductivity. These findings suggest that the BCG3 composite has a relatively low porosity or a small number of pores, resulting in enhanced conductivity.

Electrical conductivity

The conductivity values of the BCG1, BCG2, and BCG3 composites, Bi_2O_3, commercial AC and graphite are shown in Table 3. As presented in Table 3, the conductivity values of commercial AC and graphite are higher than the conductivity values of pure Bi_2O_3. Correspondingly, the conductivity values of the synthesized products were higher compared to pure Bi_2O_3, implying that the addition of AC and graphite can increase conductivity.

The composite conductivity values from the highest to the lowest were BCG3, BCG1, and BCG2. The conductivity value obtained can be related to the crystallinity of the composite produced based on the XRD results (Fig. 3). High level of composite crystallinity causes the resulting conductivity value to also be higher [31-32]. BCG2 composite has the lowest conductivity value because the crystal content of Bi_2O_3 contained in the composite was very small (see Fig. 3). The low crystallinity level of the composite caused the arrangement of the lattice between the atoms to be irregular, and the mobility of the electrons is, therefore, inhibited and the value of the electrical conductivity is low.

The BCG1 composite has a higher conductivity value than BCG2, although not too significant. This is attributed to the balanced composition of precursor materials for Bi_2O_3 formation and the addition of AC in the BCG1 composite. Consequently, Bi_2O_3 formation (as observed in Fig. 2 and 3) is uniformly distributed across the material's surface (as depicted in Fig. 5). This uniform distribution of Bi_2O_3 enhances electron mobility within the material, resulting in an increased conductivity value. Conversely, the BCG3 composite exhibits notably high conductivity because of the impurities present in the composite, according to the XRD results shown in Fig. 3.

■ CONCLUSION

Bi_2O_3/AC/graphite composites have been successfully synthesized by the hydrothermal method. The composition of the precursors used affects the formation of composites and, thus, their characteristics which can be seen from the presence of functional groups, crystal structure, morphology, surface area, pore size, and particle distribution. Additionally, identification of the thermal stability of the products formed presented different stages of thermal decomposition, although, in the end, the electrical conductivity values of the three samples do not differ significantly.

■ ACKNOWLEDGMENTS

The authors would like to thank Diponegoro University for the research funding provided through the World Class Research Universitas Diponegoro (WCRU) 2023 scheme with grant No. 118-12/UN7.6.1/PP/2021 in the fiscal year 2023.

■ AUTHOR CONTRIBUTIONS

Yayuk Astuti did the conceptualization, methodology, investigation, resources, data curation, writing, supervision, review and editing. Faradina Azahra Zaqia did the experiment, data curation, and writing draft preparation. Aulia Zahra Ekaningsih did the data curation, validation, review and editing. Gunawan did the validation, review and editing. Adi Darmawan did the validation, review and editing. All authors have read and agreed to the published version of the manuscript.

■ REFERENCES

[1] Linden, D., and Reddy, T.B., 2002, *Linden's Handbook of Batteries*, 4th Ed., McGraw-Hill Education, New York, US.

[2] Li, Y., Song, J., Ji, Y., Lu, X., Tian, Q., Chen, J., and Sui, Z., 2022, Bismuth/bismuth trioxide with a dual-

carbon support for high and long life lithium storage, *J. Phys. Chem. Solids*, 163, 110562.

[3] Ud Din, M.A., Li, C., Zhang, L., Han, C., and Li, B., 2021, Recent progress and challenges on the bismuth-based anode for sodium-ion batteries and potassium-ion batteries, *Mater. Today Phys.*, 21, 100486.

[4] Fu, H., Shi, C., Nie, J., Wang, J., and Yao, S., 2022, Bi_2O_3 nanospheres coated in electrospun carbon spheres derived Bi@C used as anode materials for lithium-ion batteries, *J. Alloys Compd.*, 918, 165666.

[5] Li, Y., Trujillo, M.A., Fu, E., Patterson, B., Fei, L., Xu, Y., Deng, S., Smirnov, S., and Luo, H., 2013, Bismuth oxide: A new lithium-ion battery anode, *J. Mater. Chem. A*, 1 (39), 12123–12127.

[6] Astuti, Y., Mei, R., Darmawan, A., Arnelli, A., and Widiyandari, H., 2022, Enhancement of electrical conductivity of bismuth oxide/activated carbon composite, *Sci. Iran*., 29 (6), 3119–3131.

[7] Astuti, Y., Musthafa, F., Arnelli, A., and Nurhasanah, I., 2022, French fries-like bismuth oxide: Physicochemical properties, electrical conductivity and photocatalytic activity, *Bull. Chem. React. Eng. Catal.*, 17 (1), 146–156.

[8] Taer, E., Taslim, R., Putri, A.W., Apriwandi, A., and Agustino, A., 2018, Activated carbon electrode made from coconut husk waste for supercapacitor application, *Int. J. Electrochem. Sci.*, 13 (12), 12072–12084.

[9] Kim, T., Jo, C., Lim, W.G., Lee, J., Lee, J., and Lee, K.H., 2016, Facile conversion of activated carbon to battery anode material using microwave graphitization, *Carbon*, 104, 106–111.

[10] Zhang, H., Yang, Y., Ren, D., Wang, L., and He, X., 2021, Graphite as anode materials: Fundamental mechanism, recent progress and advances, *Energy Storage Mater.*, 36, 147–170.

[11] Mahtab, S., Joshi, P., Arya, B., Zaidi, M.G.H., and Siddiqui, T.I., 2020, Effect of humidity on electrical conductivity of graphite nanocomposite based electrodes: A review, *Mater. Sci. Res. India*, 17 (1), 8–15.

[12] Budko, O., Butenko, O., Chernysh, O., Khomenko, V., Tverdokhlib, V., and Barsukov, V., 2022, Effect of grain composition of natural graphites on electrical conductivity of graphite-based composite materials, *Mater. Today: Proc.*, 50, 535–538.

[13] Astuti, Y., Aprialdi, F., Arnelli, A., and Haryanto, I., 2019, Synthesis of activated carbon/bismuth oxide composite and its characterization for battery electrode, *IOP Conf. Ser.: Mater. Sci. Eng.*, 509 (1), 012153

[14] Wu, C., Shen, L., Huang, Q, and Zhang, Y.C., 2011, Hydrothermal synthesis and characterization of Bi_2O_3 nanowires, *Mater. Lett.*, 65 (7), 1134–1136.

[15] Astuti, Y., Farihah, D.N., Ekaningsih, A.Z., and Darmawan, A., 2023, Electrochemical performance of one-pot hydrothermal-derived bismuth oxide/commercial activated carbon/graphite composite, *Mater. Sci. Technol.*, 39 (14), 1802–1815.

[16] Astuti, Y., Fauziyah, A., Nurhayati, S., Wulansari, A.D., Andianingrum, R., Hakim, A.R., and Bhaduri, G., 2016, Synthesis of α-bismuth oxide using solution combustion method and its photocatalytic properties, *IOP Conf. Ser.: Mater. Sci. Eng.*, 107 (1), 012006.

[17] Astuti, Y., Elesta, P.P., Widodo, D.S., Widiyandari, H., and Balgis, R., 2020, Hydrazine and urea fueled-solution combustion method for Bi_2O_3 synthesis: Characterization of physicochemical properties and photocatalytic activity, *Bull. Chem. React. Eng. Catal.*, 15 (1), 104–111.

[18] Das, D., Samal, D.P., and Meikap, B.C., 2015, Preparation of activated carbon from green coconut shell and its characterization, *J. Chem. Eng. Process Technol.*, 6 (5), 1–7.

[19] Sastrohamidjojo, H., 2018, *Dasar-dasar Spektroskopi*, Gajah Mada University Press, Yogyakarta, Indonesia.

[20] Das, T.R., Patra, S., Madhuri, R., and Sharma, P.K., 2018, Bismuth oxide decorated graphene oxide nanocomposites synthesized via sonochemical assisted hydrothermal method for adsorption of cationic organic dyes, *J. Colloid Interface Sci.*, 509, 82–93.

[21] Gondal, M.A., Saleh, T.A., and Drmosh, Q., 2012, Optical properties of bismuth oxide nanoparticles synthesized by pulsed laser ablation in liquids, *Sci. Adv. Mater.*, 4 (3-4), 507–510.

[22] Bandyopadhyay, S., and Dutta, A., 2017, Thermal, optical and dielectric properties of phase stabilized δ - Dy-Bi_2O_3 ionic conductors, *J. Phys. Chem. Solids*, 102, 12–20.

[23] Ikemoto, Y., Harada, Y., Tanaka, M., Nishimura, S., Murakami, D., Kurahashi, N., Moriwaki, T., Yamazoe, K., Washizu, H., Ishii, Y., and Torii, H., 2022, Infrared spectra and hydrogen-bond configurations of water molecules at the interface of water-insoluble polymers under humidified conditions, *J. Phys. Chem. B*, 126 (22), 4143–4151.

[24] Deng, Z., Liu, T., Chen, T., Jiang, J., Yang, W., Guo, J., Zhao, J., Wang, H., and Gao, L., 2017, Enhanced electrochemical performances of Bi_2O_3/rGO nanocomposite via chemical bonding as anode materials for lithium ion batteries, *ACS Appl. Mater. Interfaces*, 9 (14), 12469–12477.

[25] Nurdiansyah, H., and Susanti, D., 2013, Pengaruh variasi temperatur karbonisasi dan temperatur aktivasi fisika dari elektroda karbon aktif tempurung kelapa dan tempurung kluwak terhadap nilai kapasitansi electric double layer capacitor (EDLC), *J. Tek. ITS*, 2 (1), 13–18.

[26] Zhang, J., and Delichatsios, M., 2011, TGA maximum heat release rate and mass loss rate and comparison with the cone calorimeter, *Fire Saf. Sci., Proc. Int. Symp.*, 10, 1333–1346.

[27] Ma, M.G., Zhu, J.F., Sun, R.C., and Zhu, Y.J., 2010, Microwave-assisted synthesis of hierarchical Bi_2O_3 spheres assembled from nanosheets with pore structure, *Mater. Lett.*, 64 (13), 1524–1527.

[28] Klinkova, L.A., Nikolaichik, V.I., Barkovskii, N.V., and Fedotov, V.K., 2007, Thermal stability of Bi_2O_3, *Russ. J. Inorg. Chem.*, 52 (12), 1822–1829.

[29] Thommes, M., Kaneko, K., Neimark, A.V., Olivier, J.P., Rodriguez-Reinoso, F., Rouquerol, J., and Sing, K.S., 2015, Physisorption of gases, with special reference to the evaluation of surface area and pore size distribution (IUPAC Technical Report), *Pure Appl. Chem.*, 87 (9-10), 1051–1069.

[30] Agrawal, A., Janakiraman, S., Biswas, K., Venimadhav, A., Srivastava, S.K., and Ghosh, S., 2019, Understanding the improved electrochemical performance of nitrogen-doped hard carbons as an anode for sodium ion battery, *Electrochim. Acta*, 317, 164–172.

[31] Alves, A.M., Cavalcanti, S.N., da Silva, M.P., Freitas, D.M., Agrawal, P., and de Mélo, T.J.A., 2021, Electrical, rheological, and mechanical properties copolymer/carbon black composites, *J. Vinyl Addit. Technol.*, 27 (2), 445–458.

[32] Kim, M., Lee, C., and Jang, J., 2014, Fabrication of highly flexible, scalable, and high-performance supercapacitors using polyaniline/reduced graphene oxide film with enhanced electrical conductivity and crystallinity, *Adv. Funct. Mater.*, 24 (17), 2489–2499.